IEEE Photonics Journal
An IEEE Photonics Society Publication

Open Access

Vector Modulation Instability in Highly Birefringent Fibers With Circularly Polarized Eigenmodes

Volume 13, Number 1, February 2021

Kinga Zolnacz
Karol Tarnowski
Maciej Napiorkowski
Krzysztof Poturaj
Pawel Mergo
Waclaw Urbanczyk

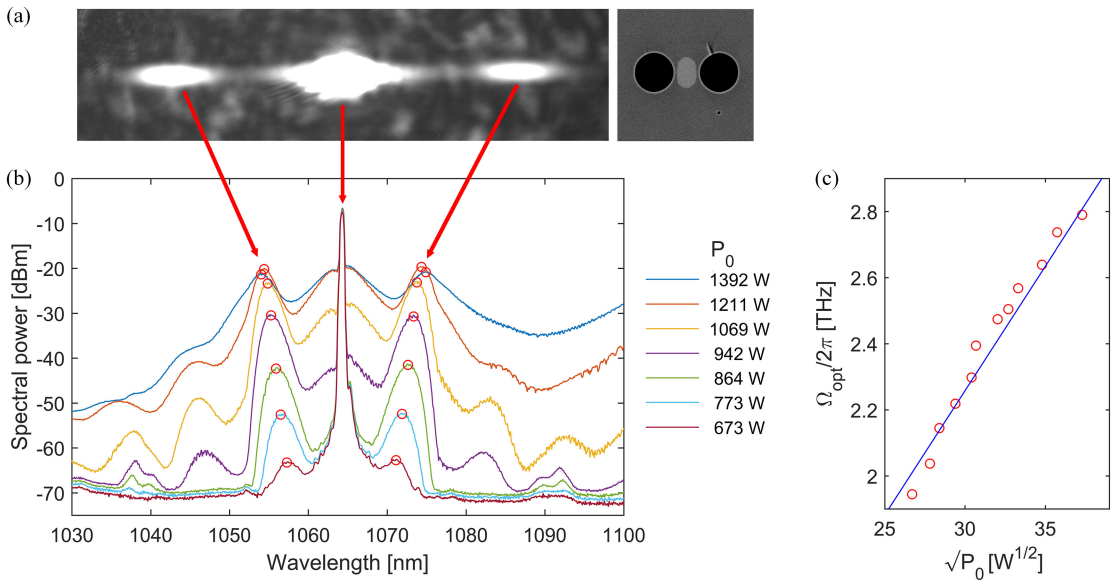

DOI: 10.1109/JPHOT.2021.3053064

Vector Modulation Instability in Highly Birefringent Fibers With Circularly Polarized Eigenmodes

Kinga Zolnacz,[1] **Karol Tarnowski**,[1] **Maciej Napiorkowski**,[1] **Krzysztof Poturaj**,[2] **Pawel Mergo**,[2] **and Waclaw Urbanczyk**[1]

[1]Department of Optics and Photonics, Faculty of Fundamental Problems of Technology, Wroclaw University of Science and Technology, 50-370 Wroclaw, Poland
[2]Laboratory of Optical Fiber Technology, Maria Curie-Sklodowska University, 20-031 Lublin, Poland

DOI:10.1109/JPHOT.2021.3053064
This work is licensed under a Creative Commons Attribution 4.0 License. For more information, see https://creativecommons.org/licenses/by/4.0/

Manuscript received September 8, 2020; revised December 18, 2020; accepted January 15, 2021. Date of publication January 20, 2021; date of current version February 3, 2021. This work was supported by the National Science Centre of Poland within grants Maestro 8 under Grant DEC-2016/22/A/ST7/00089 and Sonata Bis 8 under Grant 2018/30/E/ST7/00862. Corresponding author: Kinga Zolnacz (e-mail: kinga.zolnacz@pwr.edu.pl).

Abstract: We report a detailed study of vector modulation instability (VMI) in highly birefringent fibers with circularly polarized modes in the normal dispersion regime. We show that because of suppression of coherent terms, the VMI in circularly birefringent fibers is governed by one set of coupled-mode nonlinear Schrödinger equations regardless of the fiber birefringence. In consequence, the VMI sidebands are polarized linearly and orthogonally to the pump up to the birefringence level of 10^{-5}, similarly like in isotropic fibers. For greater birefringence the polarization states of the sidebands become elliptical with opposite handedness while the azimuth angle deviates from orthogonality to the pump. We also point on the dependence of the critical power beyond which the VMI cannot exist upon ellipticity angle θ of the eigenmodes. We show that the critical power gradually increases with the ellipticity angle and for $\theta > 17.6°$ the VMI gain is not limited, in contrast to linearly birefringent fibers. Our findings were confirmed experimentally by observation of the isotropic-like VMI in the spun side-hole fiber with nearly circularly polarized eigenmodes, in spite of relatively high birefringence of the order of 2×10^{-6}.

Index Terms: Vector modulation instability, circularly birefringent fibers, highly birefringent fibers.

1. Introduction

Vector modulation instability (VMI) is a phenomenon of generation of the spectral sidebands occurring in nonlinear birefringent fibers due to cross-phase modulation between orthogonally polarized modes under small phase and amplitude perturbations of the pump [1]. Opposite to scalar modulation instability arising only in the anomalous-dispersion regime, the VMI can be observed for either anomalous [2]–[4] or normal dispersion [5]–[15]. The VMIs were investigated in birefringent fibers with linearly polarized eigenmodes [5]–[17] and their distinct features were identified depending on the fiber birefringence. In highly birefringent fibers (group linear birefringence $\Delta N_l > 10^{-5}$), when both polarization modes are excited, the VMI generation is driven by a non-coherent nonlinear interaction between polarization modes and is called cross-phase modulation instability (XPMI)

[5]–[7], [13]–[15]. The XPMI is most efficient for the input beam polarized at 45° with respect to the fiber polarization axes and vanishes when only one polarization mode is excited. Moreover, the generated sidebands are polarized linearly, orthogonally to each other, and in parallel to the fiber polarization axes. In low-birefringence fibers (phase linear birefringence $\Delta n_l < 10^{-5}$) a coherent nonlinear interaction between polarization modes is also involved in generation of the VMI, which in this case is called polarization modulation instability (PMI). The PMI is observed when only one of the polarization modes is excited and is more efficient for the pump polarized along the slow axis [9], [10]. In this case, the PMI sidebands are polarized linearly and orthogonally to the pump. The dependence of the PMI gain spectra upon polarization state of the pump was analyzed in [11]. Finally, the PMI can also be observed in so-called isotropic fibers with very low phase birefringence ($\Delta n_l < 10^{-8}$) [16], [17] in which, similarly to weakly birefringent fibers, a coherent nonlinear interaction between the linear polarization modes is essential and the sidebands are polarized orthogonally to the pump. In an ideal case ($\Delta n_l = 0$), there are no determined polarization axes and therefore the PMI in isotropic fibers is irrespective of the azimuth of the linearly polarized input beam. When an elliptically polarized beam is introduced into the isotropic fiber, the amplitude of the sidebands gradually decays with increasing ellipticity and completely vanishes for a circularly polarized pump. This fact can be understood by expressing nonlinear propagation equations in circular polarization basis, where only incoherent and cross-phase modulation terms appear [1]. Isotropic PMI in the context of bulk nonlinear media was first discussed in 1970 [18] but due to difficulties with fabrication of perfectly isotropic fibers, it was firstly reported experimentally much later, in 1999, in a spun nearly isotropic fiber with extremely low birefringence of the order of 10^{-9} [19]. Just recently the PMIs were examined in conventional telecom fibers of different types [20].

In this paper we report on the first to our knowledge systematic study of the VMI in highly birefringent fibers with circularly polarized eigenmodes. A specific feature of circularly birefringent medium is a suppression of coherent terms in the coupled-mode nonlinear Schrödinger equations regardless of the birefringence value. Within this work, we investigate the VMI generation in such fibers by linear stability analysis of the stationary solutions of the coupled NLSE and by the numerical simulations of nonlinear light propagation. We identify several distinct features of the VMI bands in highly birefringent fibers with circularly polarized eigenmodes. These include existence of isotropic-like VMI sidebands (reported earlier for extremely low birefringence of the order of 10^{-8}) up to the group birefringence level of 10^{-5}, which are polarized linearly and orthogonally to the pump. The existence of isotropic-like VMI, in spite of relatively high birefringence, is also confirmed experimentally for spun side-hole fiber with nearly circularly polarized eigenmodes and group birefringence of the order of 2×10^{-6}. Moreover, we theoretically show that with increasing circular group birefringence beyond 10^{-5}, the polarization states of the VMI sidebands become elliptical with opposite handedness. The ellipticity angle gradually increases with the fiber group birefringence while the azimuth angle deviates from orthogonality to the pump. For high circular group birefringence (greater than 2×10^{-4}) the VMI sidebands become nearly circularly polarized. We also point on unusual behavior of the VMI in highly birefringent fibers versus ellipticity angle θ of the eigenmodes. In particular, we show that in elliptically birefringent fibers the critical power beyond which the VMI cannot exist gradually increases with θ and for $|\theta| = 17.6°$ it escapes to infinity. In contrast to linearly birefringent fibers, for ellipticity angle of the eigenmodes $|\theta| > 17.6°$, the VMI gain is not limited and increases with pump power.

2. Circularly and Elliptically Birefringent Fibers

In linearly birefringent fibers, the phase linear birefringence Δn_l represents the difference in refractive indices n_x and n_y of the two linearly and orthogonally polarized fundamental eigenmodes:

$$\Delta n_l = n_x - n_y. \tag{1}$$

Analogically, the group linear birefringence ΔN_l is defined as a difference in group refractive indices N_x and N_y and is related to the phase linear birefringence in the following way:

$$\Delta N_l = N_x - N_y = \Delta n_l - \lambda \frac{d\Delta n_l}{d\lambda}. \tag{2}$$

Birefringent fibers with elliptically or circularly polarized eigenmodes are fabricated by spinning a preform during the drawing process [21]–[23]. Twisting the fiber induces circular birefringence Δn_c which combines with its initial linear birefringence. This results in the appearance of elliptically polarized eigenmodes with opposite handedness and orthogonal azimuths, which overlap with the fiber polarization axes rotating along the fiber length with the twist pitch Λ. The elliptical birefringence induced in this way can be expressed as:

$$\Delta n = \sqrt{\Delta n_l^2 + \Delta n_c^2} - \Delta n_c, \tag{3}$$

where

$$\Delta n_c = \frac{\lambda\,|\psi|}{\pi L} = \frac{2\lambda}{\Lambda} \tag{4}$$

and ψ is the twist angle, λ is the wavelength and Λ is the twist pitch. The group elliptical birefringence is related to the phase elliptical birefringence analogically as in the case of linearly birefringent fibers, Eq. (2). After performing straightforward calculations [23], the following relation between linear and elliptical group birefringence can be derived:

$$\Delta N = \Delta n - \lambda \frac{d\Delta n}{d\lambda} = \frac{\Delta n_l}{\sqrt{\Delta n_l^2 + \Delta n_c^2}} \Delta N_l. \tag{5}$$

Finally, the ellipticity angle θ of the eigenmodes supported by a spun fiber can be expressed as:

$$\theta = 0.5\text{arctg}\left(\frac{2\lambda}{\Delta n_l \Lambda}\right). \tag{6}$$

It is known that in linearly birefringent fibers with microstructured cladding, Δn_l is highly dispersive and increases with wavelength [24]. In consequence, the dispersion term in the group modal birefringence can be so high that Δn_l and ΔN_l can differ in sign [24]. The wavelength at which the group linear birefringence crosses zero can be tuned by fiber geometry, however, as can be concluded based on Eq. 5, it cannot be changed by twisting the fiber.

To conduct the nonlinear experiments reported in Section 5, we have fabricated a special spun side-hole fiber with nearly circularly polarized modes, Fig. 1(a). The size of the elliptical core was 6.5 $\times$ 10 μm, and the dopant (GeO_2) concentration was equal to 3.8 mol%. Additionally, the reference non-twisted fiber of nearly the same geometry (drawn from the same preform) was fabricated and characterized. The measured linear phase and group birefringence in the non-twisted fiber were equal respectively to $\Delta n_l = 4.5 \times 10^{-5}$ and $\Delta N_l = -1.7 \times 10^{-5}$ at the pump wavelength $\lambda = 1064$ nm. The spun version of this fiber used in the nonlinear experiments ($\Lambda = 10$ mm) showed nearly circular birefringence, with ellipticity angle of the fundamental mode equal to $\theta = 39.3°$ and the phase and group modal birefringence equal respectively to $\Delta n = 4.3 \times 10^{-6}$ and ΔN = -2.2 $\times$ 10^{-6} at 1064 nm. These parameters have been measured using an approach described in details in [23], which combines spectral interference and lateral point-force method. Because of close vicinity of the holes to the fiber core, the linear birefringence Δn_l in the non-twisted reference fiber is highly dispersive and as a result, the group birefringence ΔN_l crosses zero at $\lambda = 970$ nm and beyond this wavelength Δn_l and ΔN_l have opposite signs. In consequence, the phase and group elliptical birefringence Δn and ΔN in the spun fiber differ in sign for $\lambda > 970$ nm [23].

A chromatic dispersion in this fiber measured using the white light interferometry method was equal to $D = -25.4$ ps/km/nm ($\beta_2 = 0.0153$ ps^2/m) at 1064 nm. The cut-off wavelength of higher order LP_{11} mode was equal to 1010 nm, however, single mode operation was assured at the pump

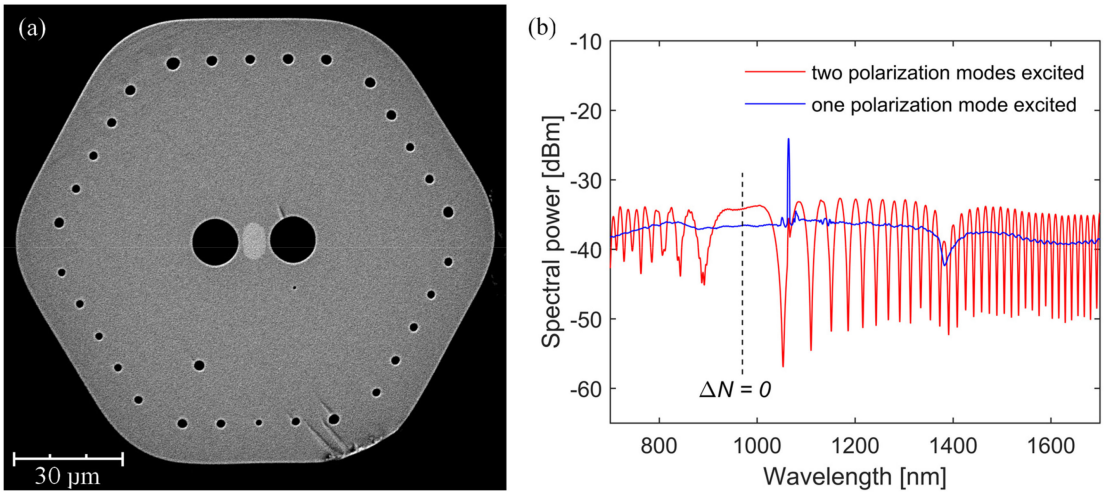

Fig. 1. (a) Cross-section of the spun side-hole fiber. Small holes in the cladding result from imperfections of the fabrication process. (b) Spectral interference fringes registered at the fiber output for the two fundamental modes excited equally (linear input polarization, red line) and for only one polarization mode excited (elliptical input polarization with $\theta = 39.3°$, blue line). Suppression of the interference fringes proves good separation of the polarization modes. The center of the widest fringe around $\lambda = 970$ nm corresponds to $\Delta N = 0$. The phase and group birefringence differ in sign beyond this wavelength.

wavelength by carefully focusing the input beam on the center of the core. In Fig. 1(b) we show the spectra registered at the output of the fiber excited with a supercontinuum source. For both polarization eigenmodes excited equally (linear input polarization) there are clearly visible high contrast interference fringes which get extinguished when only one polarization mode is excited (for elliptical input polarization with ellipticity angle $\theta = 39.3°$). This experiment proves that the birefringence in the spun side-hole fiber is high enough to prevent mixing of the nearly circularly polarized eigenmodes, in contrast to spun isotropic fibers with extremely low birefringence of the order of 10^{-8}.

3. Analysis of the VMI Gain in Circularly Birefringent Fibers

In the elliptically birefringent fiber, the right- and left-handed polarization states of the eigenmodes can be represented by the following vectors [1], [25]:

$$\mathbf{e}_r = \frac{\hat{\mathbf{x}} + ir\hat{\mathbf{y}}}{\sqrt{1+r^2}}, \mathbf{e}_l = \frac{ir\hat{\mathbf{x}} + \hat{\mathbf{y}}}{\sqrt{1+r^2}}, \tag{7}$$

where $r = \mathrm{tg}(\theta)$ and θ is the ellipticity angle ranging from 0° to 45° (where $\theta = 0°$ corresponds to linear polarization and $\theta = 45°$ to circular polarization), whereas $\hat{\mathbf{x}}$ and $\hat{\mathbf{y}}$ indicate unit vectors in the Cartesian coordinate system. In such a fiber, the nonlinear light propagation is described by the following coupled-mode NLSE [1], [25]:

$$\frac{\partial A_r}{\partial z} + \beta_{1r}\frac{\partial A_r}{\partial t} + \frac{i\beta_{2r}}{2}\frac{\partial^2 A_r}{\partial t^2} + \frac{\alpha}{2}A_r = i\gamma'\left[\left(|A_r|^2 + B|A_l|^2\right)A_r + CA_r^* A_l^2 e^{-2i\Delta\beta z}\right] + i\gamma' D\left[A_l^* A_r^2 e^{i\Delta\beta z} + \left(|A_l|^2 + 2|A_r|^2\right)A_l e^{-i\Delta\beta z}\right], \tag{8}$$

$$\frac{\partial A_l}{\partial z} + \beta_{1l}\frac{\partial A_l}{\partial t} + \frac{i\beta_{2l}}{2}\frac{\partial^2 A_l}{\partial t^2} + \frac{\alpha}{2}A_l = i\gamma'\left[\left(|A_l|^2 + B|A_r|^2\right)A_l + CA_l^* A_r^2 e^{2i\Delta\beta z}\right] + i\gamma' D\left[A_r^* A_l^2 e^{-i\Delta\beta z} + \left(|A_r|^2 + 2|A_l|^2\right)A_r e^{i\Delta\beta z}\right], \tag{9}$$

where A_r and A_l are the slowly varying envelopes of the elliptically polarized eigenmodes, β_{1r}, β_{1l} and, β_{2r}, β_{2l} are the first and second order dispersion coefficients, $\Delta\beta = \beta_r$ - β_l is proportional to the fiber phase elliptical birefringence $\Delta\beta = 2\pi\Delta n/\lambda$, α describes fiber losses, and B, C and D are the coefficients defined by the ellipticity angle θ:

$$B = \frac{2 + 2\sin^2 2\theta}{2 + \cos^2 2\theta}, C = \frac{\cos^2 2\theta}{2 + \cos^2 2\theta}, D = \frac{\sin 2\theta \cos 2\theta}{2 + \cos^2 2\theta}, \tag{10}$$

and γ' is the fiber nonlinear coefficient related to the ellipticity angle θ in the following way:

$$\gamma' = \gamma \frac{2 + \cos^2 2\theta}{3}, \tag{11}$$

where $\gamma = \omega_0 n_2/(cA_{eff})$ is the nonlinear coefficient for the linearly polarized modes, ω_0 is an angular frequency of the pump, n_2 is a nonlinear refractive index, c is the speed of light and A_{eff} is the effective mode field area. For the lossless fiber ($\alpha = 0$) with circularly polarized eigenmodes ($\theta = 45°$) the coefficients B, C, D take the following values $B = 2$, $C = 0$, $D = 0$. Consequently the coherent terms proportional to C and D in the coupled-mode NLSE (Eqs. (8) and (9)) vanish, which leads to the following simplification:

$$\frac{\partial A_+}{\partial z} + \frac{\Delta\beta_1}{2}\frac{\partial A_+}{\partial t} + \frac{i\beta_{2+}}{2}\frac{\partial^2 A_+}{\partial t^2} = i\gamma'\left(|A_+|^2 + B|A_-|^2\right)A_+, \tag{12}$$

$$\frac{\partial A_-}{\partial z} - \frac{\Delta\beta_1}{2}\frac{\partial A_-}{\partial t} + \frac{i\beta_{2-}}{2}\frac{\partial^2 A_-}{\partial t^2} = i\gamma'\left(|A_-|^2 + B|A_+|^2\right)A_-, \tag{13}$$

where A_+ and A_- are the slowly varying envelopes of the right- and left-handed circularly polarized eigenmodes, and $\Delta\beta_1 = \beta_{1+} - \beta_{1-} = \Delta N/c$ is the group velocity mismatch of the polarization modes for the time frame chosen to travel with the average velocity $\Delta\beta_{1\mathrm{av}} = (\beta_{1+} + \beta_{1-})/2$. Although the circular phase birefringence is not directly present in the set of above equations, it is related to the phase terms, which were factored out to obtain slowly varying envelopes. These phase terms are different in both equations, namely exp(i$\beta_+ z$) in the first equation and exp(i$\beta_- z$) in the second one, where β_+ and β_- denote the modes propagation constants at pump frequency. In other words, the circular phase birefringence, which is directly related to the difference in propagation constants $\Delta\beta = \beta_+$ - β_-, is indirectly present in the above equations set.

Equations (12) and (13) describe the interaction of two copropagating orthogonally polarized waves at the same wavelength in the circularly birefringent fiber. This set of equations is referred in literature as the set of incoherently coupled nonlinear Schrodinger equations (ICNLS) – as the coherent coupling terms vanish. Initially, this set of equations had been considered by Agrawal in [26] for two copropagating waves at different wavelengths, where the coherent coupling terms had been disregarded. The importance of the coherent coupling terms for dual wavelength pumping was pointed by Rothenberg [27] and further discussed and studied experimentally in [28]–[30]. The same equations also rule PMI in highly linearly birefringent fibers. In this case, $B = 2/3$ [15] and the coherent coupling terms are disregarded because of high linear phase birefringence. It should be stressed, however, that in circularly birefringent fibers the coherent coupling terms vanish because the coefficients C and D are equal to zero and no approximation is needed to remove them from the NLSE.

The steady-state solutions of the above coupled-mode NLSE under small perturbation $\alpha_\pm(z,t)$ of the pump can be expressed as [26]:

$$A_\pm(z,t) = \left[\sqrt{P_\pm} + a_\pm(z,t)\right]\exp\left(i\phi_\pm(z)\right), \tag{14}$$

where $P_\pm$ is the power in the respective circularly polarized mode and $\phi_\pm(z) = \gamma'(P_\mp + BP_\pm)z$ is the nonlinear phase shift. Assuming that:

$$a_\pm = u_\pm \exp[i(Kz - \Omega t)] + iv_\pm \exp[-i(Kz - \Omega t))], \tag{15}$$

where K is the wave number and Ω is the angular frequency of perturbation, it is possible to derive the following dispersion relation by linearizing Eqs. (12) and (13) with respect to a_+ and a_- [6], [26]:

$$\left[(K-b)^2 - H_+\right]\left[(K+b)^2 - H_-\right] = C^2, \tag{16}$$

where

$$b = \frac{\Omega \Delta\beta_1}{2} = \frac{\Omega \Delta N}{2c}, \tag{17}$$

$$H_\pm = \frac{\beta_{2\pm}\Omega^2}{2}\left(\frac{\beta_{2\pm}\Omega^2}{2} + 2\gamma' P_\pm\right), \tag{18}$$

and

$$C = B\Omega^2\gamma'\sqrt{\beta_{2+}\beta_{2-}P_+P_-}. \tag{19}$$

The VMI is observed only when K takes imaginary values and the spectral dependence of the VMI gain is given by the following relation:

$$g(\Omega) = 2\mathrm{Im}(K). \tag{20}$$

Providing that the two polarization modes have the same dispersion $\beta_{2+} = \beta_{2-} = \beta_2$ and are equally excited $P_+ = P_- = P_0/2$, the dispersion relation can be simplified to the following form:

$$K = \sqrt{H + b^2 \pm \sqrt{4Hb^2 + C^2}}. \tag{21}$$

One should note that because of vanishing of the coherent terms in the couple-mode NLSE for circularly polarized modes, the above dispersion equation and its solutions are independent of the fiber phase elliptical birefringence Δn. In case of weakly birefringent fibers ($\Delta N < 10^{-5}$), one can assume that $b \approx 0$, which leads to further simplification:

$$K = \sqrt{H \pm C}, \tag{22}$$

and consequently

$$g(\Omega) = \beta_2\sqrt{\Omega^2\left({\Omega_c}^2 - \Omega^2\right)}, \tag{23}$$

where

$$\Omega_c = \sqrt{\frac{4\gamma}{3\beta_2}}\sqrt{P_0} \tag{24}$$

is the cut-off angular frequency beyond which the VMI does not occur and for γ' we substituted $\gamma' = 2\gamma/3$. The optimal detuning angular frequency corresponding to the maximum gain is given by:

$$\Omega_{opt} = \sqrt{\frac{2\gamma}{3\beta_2}}\sqrt{P_0} \tag{25}$$

In spite of relatively high group birefringence ($\Delta N < 10^{-5}$), the derived relations for Ω_{opt} and Ω_c are the same as in case of isotropic fibers ($\Delta N < 10^{-8}$). This happens because in both cases the coherent terms in the coupled-mode NLSE are extinguished either by zero phase modal birefringence [16], [17] or by circular polarization of the eigenmodes. Therefore, we conclude that the observation of isotropic-like VMI in spun fibers does not prove their extremely low birefringence but only indicates that the eigenmodes have the polarization states close to circular.

Another interesting feature of the VMI in spun birefringent fibers can be observed in the regime of high birefringence ($\Delta N > 10^{-5}$). In this case, the coherent terms in Eqs. (8) and (9) can be disregarded because they oscillate fast with propagation distance which makes it possible to analyze the impact of the mode ellipticity represented by the coefficient B on the VMI generation. It

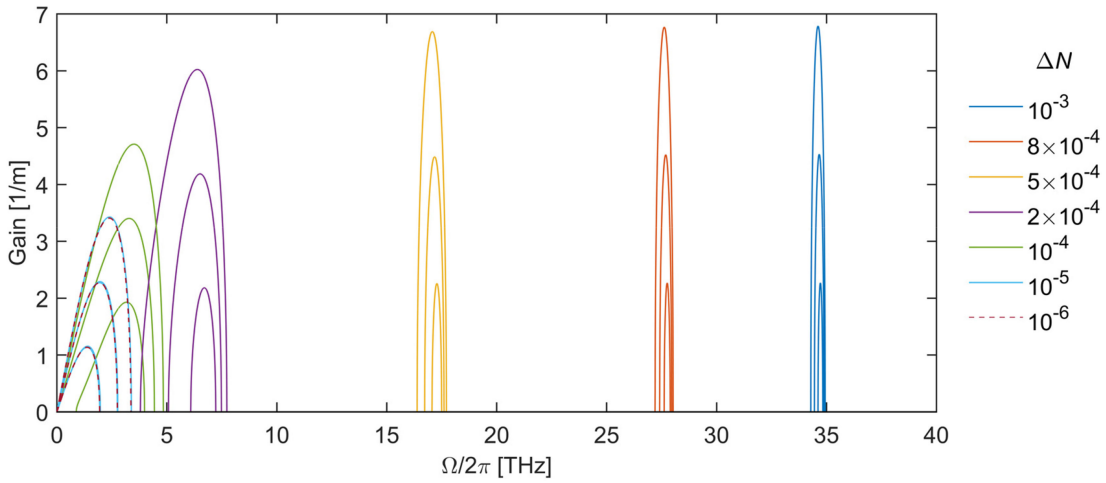

Fig. 2. Frequency dependence of the VMI gain for $P_0 = 500$, 1000 and 1500 W (from bottom to top) for different group birefringence values ΔN.

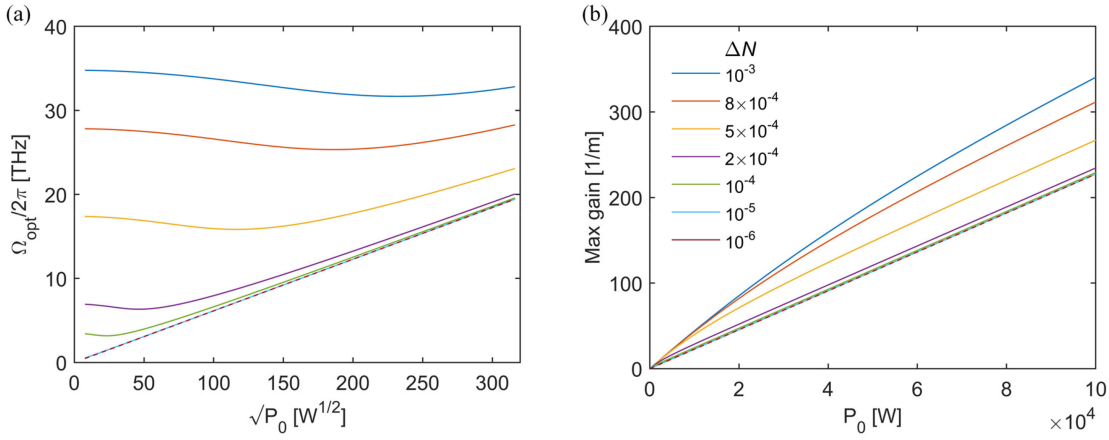

Fig. 3. (a) Optimal detuning frequency as a function of square root of pump power and (b) maximal gain vs. pump power calculated for circularly birefringent fiber ($B = 2$) for different values of group birefringence ΔN. The results obtained for $\Delta N \leq 10^{-5}$ are nearly identical as for the isotropic fiber ($\Delta N = 0$).

is known that in highly birefringent fibers with linearly polarized eigenmodes, the bandwidth of the VMI decreases and shifts to lower frequency as the pump power increases. Moreover, there exists a critical pump power P_c depending upon the group velocity mismatch of the polarization modes, above which the VMI gain ceases [6]. Based on the dispersion relation, Eq. (21), it is possible to derive more general formula for the critical power in elliptically polarized spun fibers which includes the modes ellipticity:

$$P_c = \frac{3\Delta\beta_1{}^2}{4\beta_2\gamma\left(1 - 3\sin^2 2\theta\right)}. \tag{26}$$

The above expression shows that for $\sin^2 2\theta = 1/3$ ($\theta = 17.6°$), which corresponds to $B = 1$, the critical power escapes to infinity and for $B > 1$ the gain is not limited and increases with the pump power, Figs. 2–3. Such behavior is qualitatively different than in case of linearly birefringent fibers ($B = 2/3$) and allows for much more efficient generation of the VMI in elliptically birefringent fibers with $\theta > 17.6°$.

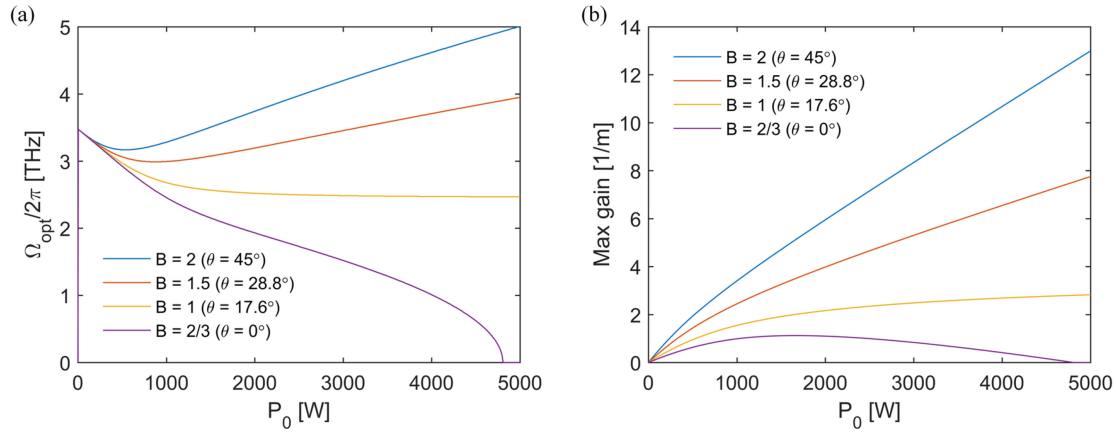

Fig. 4. (a) Optimal detuning frequency and (b) maximal gain calculated vs. pump power for different coefficients B and group birefringence $\Delta N = 10^{-4}$.

The dependence of the critical power P_c upon modes ellipticity θ can be explained in terms of phase-matching of the four-wave-mixing process, in which two pump photons are converted to two photons detuned in angular frequency by Ω and $-\Omega$. The maximum of four-wave-mixing gain arises when the three terms, namely: group velocity dispersion, group birefringence and nonlinearity, contributing to the phase mismatch mutually compensate. The initial phase mismatch for frequency shifted waves occurs due to normal group velocity dispersion. This mismatch can be compensated by the group birefringence contribution which is negative. Finally, the nonlinear contribution (which accounts for self-phase modulation and cross-phase modulation) adds up to the overall mismatch in birefringent fibers. In linearly birefringent fibers, beyond certain power level, the nonlinear term exceeds the negative contribution from the group birefringence and obtaining the phase matching is no longer possible. It means that for a given birefringence level there exists a critical power beyond which the gain of the VMI vanishes. However, in elliptically birefringent fibers, the sign of the nonlinear contribution to the phase matching condition depends on the coefficient B. The nonlinear contribution cancels when $B = 1$ and takes negative values for $B > 1$. Consequently for $B > 1$ the pump power does not longer limit the VMI gain.

It can be also noted that for highly birefringent fiber with elliptically polarized eigenmodes with ellipticity of $\theta = 17.6°$, the coupled NLSE system (Eqs. (8) and (9)) takes the form of the integrable Manakov equations [25, 31] (a different value of the ellipticity angle in reference [25] – approximately 35° – is due to a different definition of the ellipticity angle). The VMI was investigated experimentally in the Manakov fiber system in dual pump configuration [32]. However, in this work the coupled NLSE system reduces to Manakov equations due to random and rapid changes in birefringence orientation [33], what differs qualitatively from the reduction resulting from the eigenmodes ellipticity in highly birefringent fibers considered in our work.

In Fig. 4 we show the optimal frequency and the maximal gain calculated as a function of pump power for group birefringence equal to 10^{-4} and coefficients $B = 2$, 1.5, 1 and 2/3. Similarly as it is in the linearly birefringent fibers, the Ω_{opt} at low power limit is defined by the ratio of group birefringence and fiber dispersion:

$$\Omega_{opt} = \frac{\Delta\beta_1}{\beta_2} = \frac{\Delta N}{c\beta_2}, \tag{27}$$

and is independent of the modes ellipticity. Moreover, as it is shown in Fig. 3(a), in fibers with high birefringence, the Ω_{opt} initially shifts towards lower frequencies with increasing pump power P_0 but for high powers it asymptotically approaches linear increase with proportionality coefficient between Ω_{opt} and $\sqrt{P_0}$ the same as in the case of isotropic fibers. All the calculations presented in

Figs. 2–8 were conducted for the parameters as in the fabricated spun fiber shown in Fig. 1, i.e., $A_{eff} = 45\ \mu m^2$, $n_2 = 2.6 \times 10^{-20}$ m^2/W, $\lambda_0 = 1064$ nm, $\gamma = 0.00341$ W^{-1}/m, $\beta_2 = 0.0153$ ps^2/m.

4. Numerical Analysis of the Polarization Evolution in the VMI Sidebands

In this section, we present the results of numerical simulations performed to support and confirm the theoretical results obtained by the linear stability analysis. Moreover, the numerical simulations allowed us to better visualize the evolution of the polarization state along propagation distance, including rotation of the polarization azimuth. We performed the simulations based on the set of coupled-mode NLSE (Eqs. (12) and (13)), which was solved with the standard split-step Fourier method [1] introducing one-photon per mode noise [34].

We recall here that the circular phase birefringence is indirectly present in the set of coupled-mode NLSE through the different phase factors used in the two equations. Those equations could be rewritten to have the same phase factor with the following substitutions:

$$A_{\pm} = A'_{\pm} \exp\left(\mp i \frac{\Delta\beta_0}{2}\right). \tag{28}$$

Therefore, the equivalent equations set takes the following form:

$$\frac{\partial A'_+}{\partial z} - \frac{i\Delta\beta_0}{2} A'_+ + \frac{\Delta\beta_1}{2}\frac{\partial A'_+}{\partial t} + \frac{i\beta_{2+}}{2}\frac{\partial^2 A'_+}{\partial t^2} = i\gamma'\left(\left|A'_+\right|^2 + B\left|A'_-\right|^2\right) A'_+, \tag{29}$$

$$\frac{\partial A'_-}{\partial z} + \frac{i\Delta\beta_0}{2} A'_- - \frac{\Delta\beta_1}{2}\frac{\partial A'_-}{\partial t} + \frac{i\beta_{2-}}{2}\frac{\partial^2 A'_-}{\partial t^2} = i\gamma'\left(\left|A'_-\right|^2 + B\left|A'_+\right|^2\right) A'_-. \tag{30}$$

The transfer between the two representations using A_+ and A_- or A'_+ and A'_- is straightforward.

In all simulations, we assumed that the pump at the fiber input is linearly polarized along x-axis and we fixed the pump power at 1000 W. We analyzed the growth of the VMI bands on the propagation distance equal to 6 m. In the following figures, we present the calculated spectra in circular polarizations basis and in linear polarizations basis. We have also calculated the azimuth angle ϕ and ellipticity angle θ in the VMI bands. The evolution of these two parameters is shown over the last meter of the fiber length, since at this distance the VMI bands have already built up. Finally, we show also the polarization state of light at Ω_{opt} at the fiber output as a function of group birefringence ΔN.

We started the simulations with the isotropic fiber: $\Delta N = 0$ and $\Delta n = 0$ (Fig. 5(a)). As expected, the VMI bands are linearly polarized ($\theta = 0°$) and appear only in y-axis (i.e., orthogonally to the pump). Introduction of nonzero phase birefringence ($\Delta n = 10^{-6}$) modifies this picture (Fig. 5(b)). The VMI bands are linearly polarized and orthogonally to the pump, but the polarization state in the whole spectrum rotates along the propagation distance due to circular birefringence of the fiber. This rotation is visible as fringes in the spectra displayed in linear basis and in evolution of the azimuth angle. The rotation is also revealed in Figs. 5(c) and 5(d) showing the evolution of the azimuth angles at pump frequency ($\Omega = 0$ THz) and in the VMI band (at $\Omega_{opt}/2\pi = 1.9$ THz) for zero and nonzero phase birefringence. Numerical simulations confirm that the position and gain in the VMI bands are not influenced by nonzero phase birefringence. Moreover, the position of the VMI bands agrees with Ω_{opt} determined by the linear stability analysis.

In the next step, we have analyzed the fiber with significant group birefringence $\Delta N = 10^{-4}$. In this case (Fig. 6), the VMI bands are no longer linearly polarized, they are more shifted with respect to the pump and their maximal gain is higher than for $\Delta N = 0$. Moreover, our simulations show that the ellipticity angle θ is frequency depended within the VMI bands, i.e., it increases with frequency detuning (Figs. 6(a) and 6(b)). The polarization azimuth ϕ in the VMI bands is no longer perpendicular to the pump what can be seen in Fig. 6(c) for $\Omega_{opt}/2\pi = 3.3$ THz. As in the previous case, the nonzero phase birefringence results only in rotation of the polarization states of the VMI bands and the pump with the propagation distance (Fig. 6(d)).

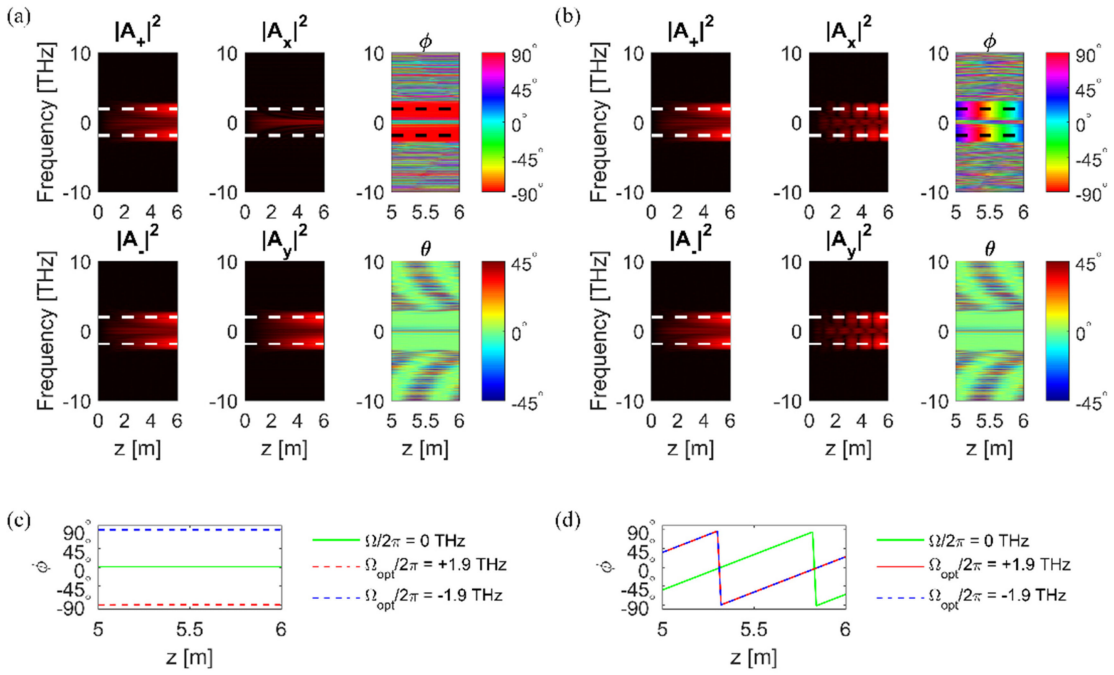

Fig. 5. (a) Growth of the VMI bands in the fiber with zero group birefringence $\Delta N = 0$ and zero phase birefringence $\Delta n = 0$ and (b) with phase birefringence $\Delta n = 10^{-6}$. (c) Evolution of the polarization azimuth angle over the last meter of the fiber calculated for $\Delta N = 0$ and $\Delta n = 0$ and (d) $\Delta n = 10^{-6}$. Spectra are presented in circular and linear polarizations basis. The white dashed lines indicate $\pm\Omega_{opt}/2\pi = 1.9$ THz. The right color panels show the evolution of the polarization azimuth ϕ and ellipticity θ angles over the last meter of the fiber. The black dashed lines indicate the cross sections presented in (c) and (d).

We have also analyzed the nonlinear propagation in the fiber with high group birefringence $\Delta N = 2 \times 10^{-4}$ (Fig. 7). In this case, the VMI bands are more spectrally shifted with respect to the pump and their maximal gain is greater than for $\Delta N = 10^{-4}$. Moreover, the simulations show that the VMI bands are almost circularly polarized with constant ellipticity angle across the bands.

Finally, we show the azimuth and the ellipticity angles at $\Omega_{opt}/2\pi$ calculated for different group birefringence and zero phase birefringence, Fig. 8. In this way, we can observe a transition between two extreme situations. For small group birefringence ($\Delta N < 10^{-5}$), the VMI bands are nearly linearly polarized with the azimuth orthogonal to the pump, similarly as it is in isotropic fibers. With increasing ΔN the polarization state in the VMI bands becomes elliptical with gradually increasing ellipticity angle θ and opposite handedness. For high group birefringence ($\Delta N > 2 \times 10^{-4}$), the VMI bands approach circular polarization ($\theta > 40°$). The polarization azimuth of the elliptically polarized side-bands is orthogonal to the pump in the regime of small group birefringence ($\Delta N < 10^{-5}$) and gradually deviates from orthogonality with increasing ΔN. This deviation has the same absolute value in both bands, but its sign is opposite. It reveals the interplay between newly conversed light (at given propagation distance) which is orthogonal to the pump (at this distance), and already coupled light with azimuth rotating with different angular velocity than the pump.

5. Experiment

To experimentally observe the VMI in the birefringent medium with circularly polarized eigenmodes, we have used the six-meter long fiber described in Section 2, pumped with Nd:YAG pulse laser, $\lambda_0 = 1064.3$ nm, pulse duration of 600 ps, repetition rate of 20 kHz and peak power close to 2500 W

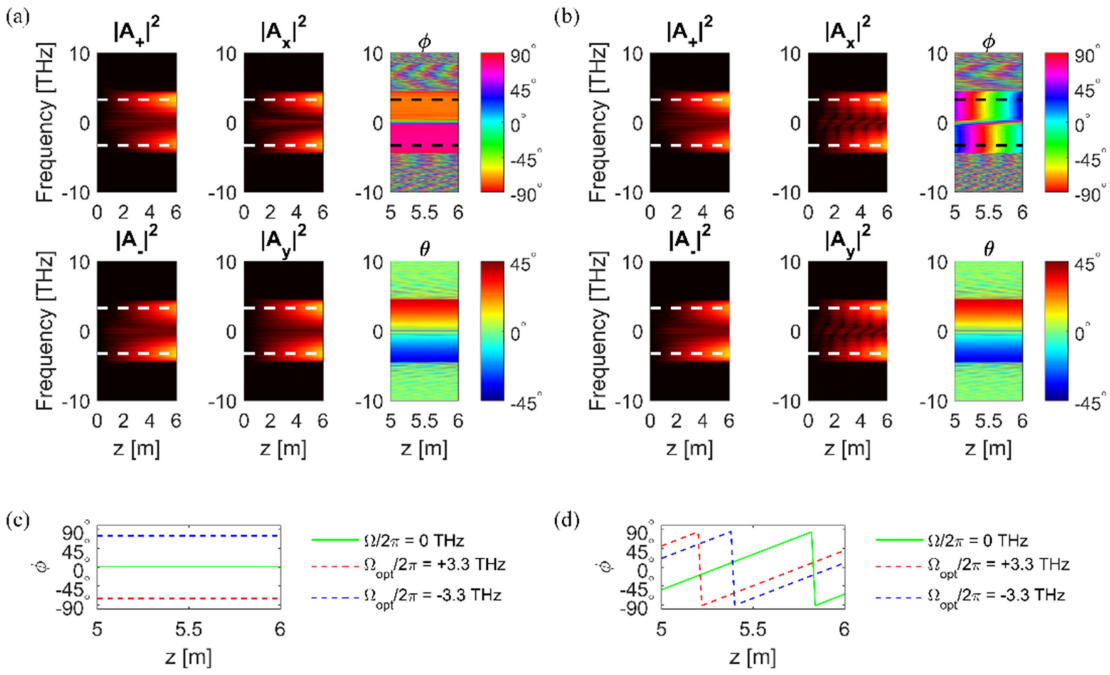

Fig. 6. (a) Growth of the VMI bands in the fiber with significant group birefringence $\Delta N = 10^{-4}$ and zero phase birefringence $\Delta n = 0$ and (b) with phase birefringence $\Delta n = 10^{-6}$. (c) Evolution of the polarization azimuth angle over the last meter of the fiber calculated for $\Delta N = 10^{-4}$ and $\Delta n = 0$ and (d) $\Delta n = 10^{-6}$. Spectra are presented in circular and linear polarizations basis. The white dashed lines indicate $\pm\Omega_{opt}/2\pi = 3.3$ THz. The right panels show the evolution of the polarization azimuth ϕ and ellipticity θ angles over the last meter of the fiber. The black dashed lines indicate the cross sections presented in (c) and (d).

(determined knowing average power measured with power meter, pulse duration and modulation frequency). Rotatable polarizers, quarter-wave plates and half-wave plates were employed to control the light polarization at the fiber input/output. The fiber supports two spatial modes at 1064 nm, however, the LP_{11} mode was extinguished by focusing the exciting beam on the center of the core. The coupling efficiency of the pump laser beam to the fundamental mode of the fiber was equal to 65%. In Fig. 9, we show the output signal spectrally decomposed in horizontal direction (for the elliptical fiber core oriented vertically) by a diffraction grating with 600 lines/mm and registered by a CMOS camera. This picture clearly shows that both the pump and the generated VMI sidebands propagate in the fundamental modes.

The spectra registered for different peak powers P_0 of the pump pulses introduced into the fiber, varied by the linear gray filter placed at the fiber input, are shown in Fig. 9(b). For the peak power greater than 900 W, higher order VMI peaks were generated in the cascaded process. The spectral position of the maximal gain λ_{opt} for the first order VMI is marked by circles. The corresponding optimal frequency detuning $\Omega_{opt}/2\pi$ of the generated sidebands as a function of $\sqrt{P_0}$is shown in Fig. 9(c). As can be seen, $\Omega_{opt}/2\pi$ is a linear function of the $\sqrt{P_0}$ which is a characteristic feature of isotropic PMI, however, as shown by our analysis, in case of circularly polarized modes this type of dependence can be also observed in fibers with significant circular birefringence reaching 10^{-5}.

For perfect circular polarization of the fiber eigenmodes, the gain of the VMI is maximal for linearly polarized pump and insensitive to the azimuth of linear polarization. In Fig. 10(a), we show the registered spectra for different orientations of the linearly polarized pump of peak power $P_0 = 1000$ W (azimuth 0° indicates that the electric vector of the pump was in parallel to the longer axes of the elliptical core). Because the fiber eigenmodes are not perfectly circularly polarized, the

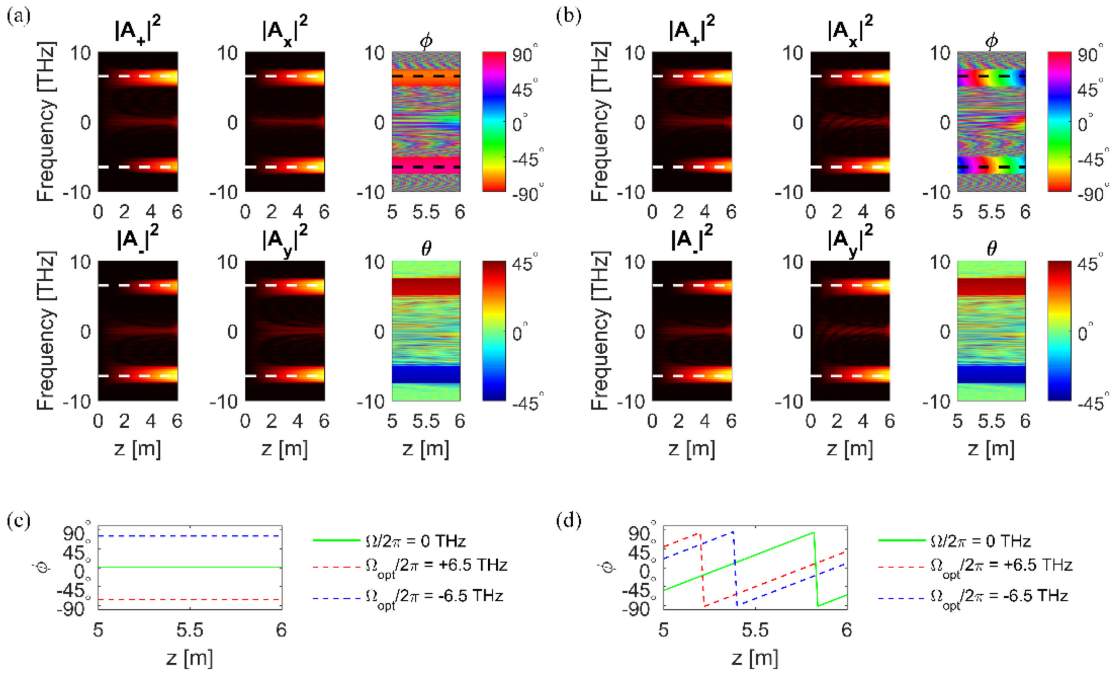

Fig. 7. (a) Growth of the VMI bands in the fiber with a high group birefringence $\Delta N = 2 \times 10^{-4}$ and zero phase birefringence $\Delta n = 0$ and (b) with phase birefringence $\Delta n = 10^{-6}$. (c) Evolution of the polarization azimuth angle over the last meter of the fiber calculated for $\Delta N = 2 \times 10^{-4}$ and $\Delta n = 0$ and (d) $\Delta n = 10^{-6}$. Spectra are presented in circular and linear polarizations basis. The white dashed lines indicate $\pm\Omega_{opt}/2\pi = 6.5$ THz. The right panels show the evolution of the polarization azimuth ϕ and ellipticity θ angles over the last meter of the fiber. The black dashed lines indicate the cross sections presented in (c) and (d).

gain of the VMI is slightly dependent on the azimuth of linearly polarized pump, with maximum reached for the linear polarization aligned in parallel to longer axis of the core, which privileges the excitation of the slower mode (with greater effective index) of elliptical polarization. This effect is most probably caused by coherent terms in the coupled-mode NLSE, Eqs. (8) and (9), which are not completely extinguished for the ellipticity angle $\theta = 39.3°$ for which $B = 1.92$, $C = 0.02$ and $D = 0.09$. Indeed, the analysis of the VMI efficiency conducted in [8] for linearly birefringent fibers with coherent terms included shows that the excitation of the slower mode enhances the VMI generation.

The dependence of the VMI gain upon the ellipticity angle of the pump was measured for $P_0 = 1000$ W by rotating a quarter-wave plate placed at the fiber input, starting from $\theta = 0°$ (linear polarization with electric vector parallel to the longer axis of the core) to $\theta = 45°$ (circular right handed polarization) with the step of 5°. As it is shown in Fig. 10(b), the effectiveness of the sidebands generation decreases with increasing ellipticity of the pump and for $\theta > 35°$, i.e., close to the circular polarization of the pump, the VMI sidebands disappear completely, similarly like in isotropic fibers [19]. This behavior is symmetrical with respect to the handedness of elliptical polarization of the pump. The dependence of the VMI gain upon pump ellipticity can be explained based on Eq. 21, which shows that the gain is proportional to $\sqrt{P_+P_-} = 0.5P_0\cos(2\theta)$. This term reaches the maximum value for linearly polarized pump ($\theta = 0°$) and vanishes for circularly polarized pump ($\theta = \pm 45°$).

Finally, we have also investigated the polarization state of the generated VMI sidebands. In this experiment the pump was linearly polarized at the fiber input and the polarization state of the sidebands was analyzed at the fiber output with the use of a polarizer. As the linear polarization of

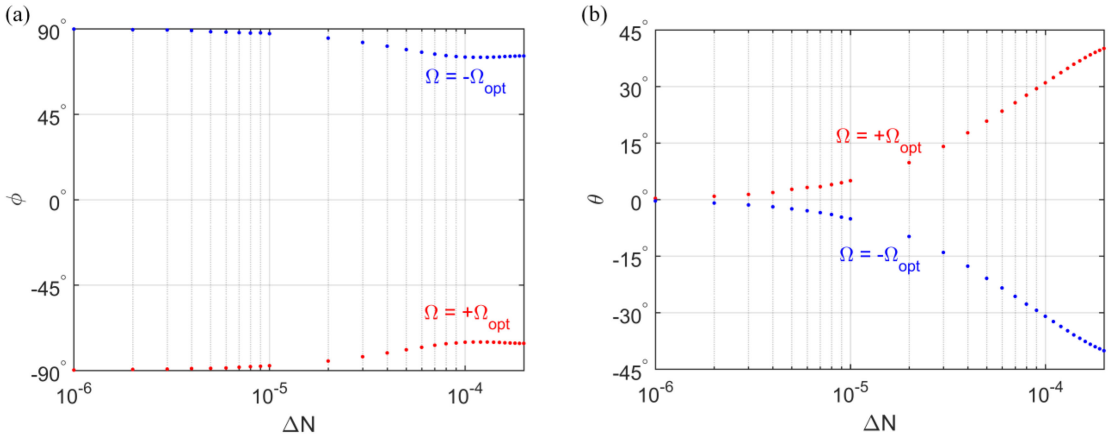

Fig. 8. Evolution of the azimuth ϕ and ellipticity θ angles calculated at Ω_{opt} as a function of the fiber group birefringence.

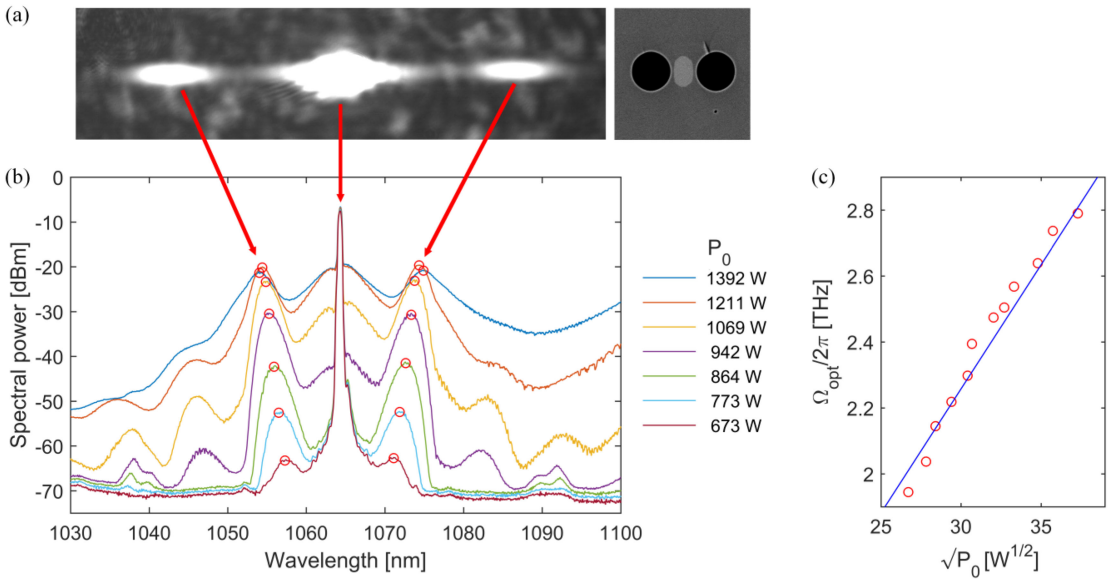

Fig. 9. (a) Output signal spectrally decomposed by diffraction grating in horizontal direction for vertical orientation of the elliptical core showing that the pump and the VMI sidebands propagate in the fundamental mode. (b) Spectra registered for different peak pump powers P_0 with the maxima of the first order sidebands marked with circles. (c) Optimal detuning frequency of the first order VMI sidebands as a function of square root of the pump power measured (circles) and calculated according to Eq. (25) (line).

the pump rotates along the fiber length due to circular birefringence, the pump azimuth at the fiber output was used as the reference direction to determine the polarization azimuths of the sidebands. First, by rotating the analyzer we have extinguished the pump at the fiber output for low excitation power to avoid any polarization changes induced by nonlinear effects. Then, the pump power was increased to level of $P_0 = 1000$ W allowing to observe the VMI sidebands and to analyze their polarization states. In Fig. 11, we show two spectra registered for the transmission azimuth of the polarizer at the fiber output set in parallel to the azimuth of the pump and rotated by 90°. This experiment proves that the sidebands are polarized linearly and the azimuths of the odd orders are

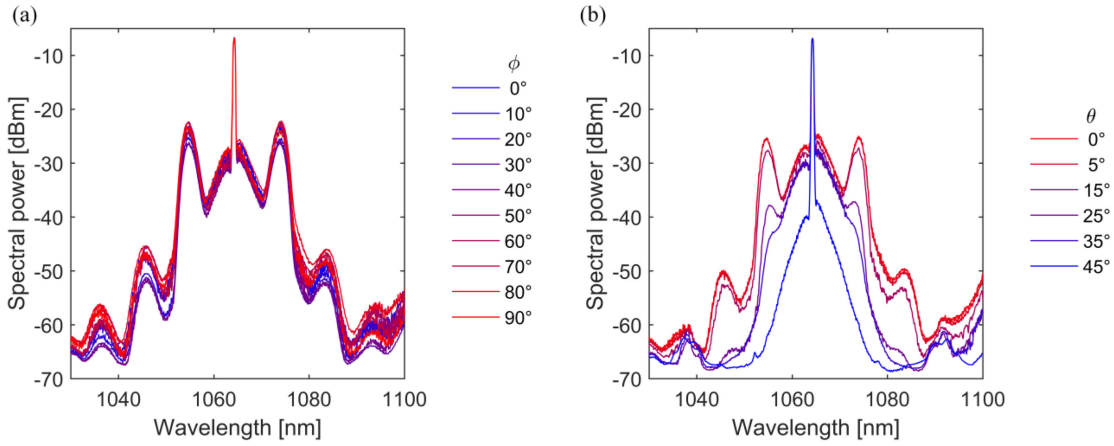

Fig. 10. (a) Dependence of the VMI spectra upon azimuth ϕ of the linearly polarized pump and (b) ellipticity angle θ of the pump. Azimuth 0° indicates that the electric vector of the pump was parallel to the longer axis of the fiber core. The longer axis of the polarization ellipse of the pump was kept constant and in parallel to the longer axis of the fiber core.

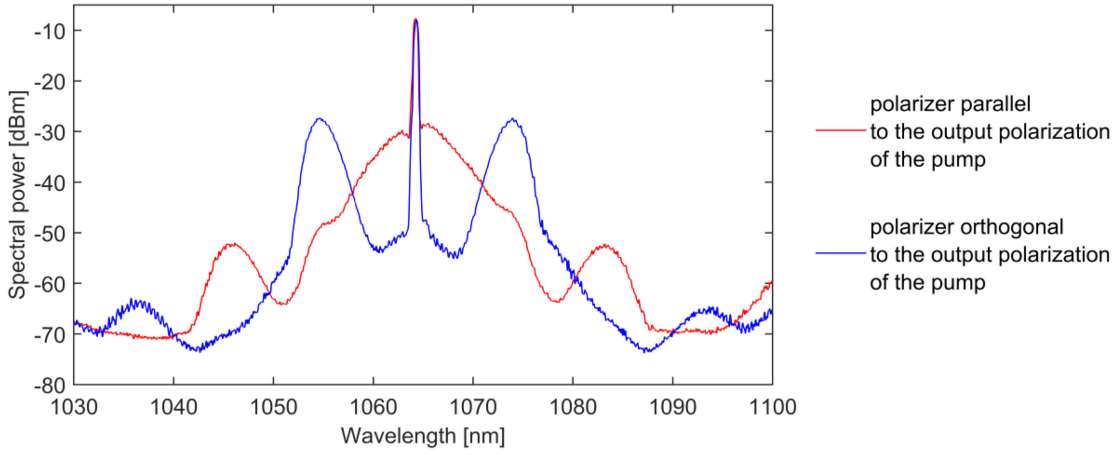

Fig. 11. The VMI sidebands registered after passing through the polarizer placed at the fiber output and aligned in parallel (red) and perpendicularly (blue) to the output polarization azimuth of the pump.

perpendicular while the even orders are parallel to the pump. The same polarization features are observed for the PMI sidebands generated in isotropic fibers [19].

6. Conclusion

In conclusions, we have experimentally demonstrated that the VMI in a nearly circularly birefringent spun fiber, in spite of quite significant birefringence $\Delta N = -2.2 \times 10^{-6}$, shows polarization behavior typical for isotropic PMI. Therefore, the existence of isotropic-like VMI in spun fibers does not prove their extremely low birefringence but only indicates that the eigenmodes have polarization states close to circular. This experimental observation is in agreement with the results of the analysis based on the coupled-mode NLSE for circularly polarized modes proving that the VMIs in fibers with circular birefringence up to the level of 10^{-5} behave similarly to the PMI in isotropic fibers.

Moreover, we have theoretically shown that in case of the spun fibers with high birefringence (exceeding 10^{-4}), which suppresses the coherent terms in the coupled-mode NLSE, the VMI gain shows distinct behavior versus ellipticity of the fiber modes. For small ellipticity angle $0 \leq |\theta| \leq 17.6°$ which corresponds to $2/3 \leq B \leq 1$, the gain is extinguished to zero for the pump power exceeding certain critical value. For greater ellipticity, the critical power ceases to exist and the gain increases monotonically with the pump power. This effect is related to relative strength of the self-phase modulation and cross-phase modulation defined by the coefficient B. For $B > 1$ ($|\theta| > 17.6°$) the XPMI starts to dominate and the VMI gain is no longer limited. Our analysis therefore shows that the VMI may be more efficiently generated in elliptically birefringent fibers with modes ellipticity $|\theta| > 17.6°$ than in fibers with linear birefringence. This effect can be exploited to seed other nonlinear phenomena like generation of ultrashort pulse trains or generation of supercontinuum in birefringent fibers with nearly circularly polarized modes.

Finally, we have also numerically analyzed the evolution of the polarization state in the VMI bands versus group circular birefringence. For small birefringence ($\Delta N < 10^{-5}$), similarly like in isotropic fibers, the VMI bands are polarized linearly and orthogonally to the pump. With increasing group birefringence, the polarization states of the sidebands become elliptical with opposite handedness. The ellipticity angle gradually increases with the fiber group birefringence while the azimuth angle deviates from orthogonality to the pump. For high circular birefringence, the VMI sidebands become circularly polarized.

References

[1] G. P. Agrawal, *Nonlinear Fiber Optics*, 6th ed., New York; Orlando, FL; San Diego, CA: Academic Press, 2019, Chap. 6.

[2] B. Kibler, C. Billet, J. M. Dudley, R. S. Windeler, and G. Millot, "Effects of structural irregularities on modulational instability phase matching in photonic crystal fibers," *Opt. Lett.*, vol. 29, no. 16, pp. 1903–1905, 2014.

[3] D. Amans, E. Brainis, M. Haelterman, P. Emplit, and S. Massar, "Vector modulation instability induced by vacuum fluctuations in highly birefringent fibers in the anomalous-dispersion regime," *Opt. Lett.*, vol. 30, pp. 1051–1053, 2005.

[4] A. T. Nguyen *et al.*, "Enhanced cross phase modulation instability in birefringent photonic crystal fibers in the anomalous dispersion regime," *Opt. Exp.*, vol. 14, pp. 8290–8297, 2006.

[5] P. D. Drummond, T. A. B. Kennedy, J. M. Dudley, R. Leonhardt, and J. D. Harvey, "Cross-phase modulational instability in high-birefringence fibers," *Opt. Commun.*, vol. 78, no. 2, pp. 137–142, 1990.

[6] J. E. Rothenberg, "Modulational instability for normal dispersion," *Phys. Rev. A*, vol. 42, no. 1, pp. 682–685, 1990.

[7] A. Kudlinski *et al.*, "Simultaneous scalar and cross-phase modulation instabilities in highly birefringent photonic crystal fiber," *Opt. Exp.*, vol. 21, no. 7, pp. 8437–8443, 2013.

[8] S. Wabnitz, "Modulational polarization instability of light in a nonlinear birefringent dispersive medium," *Phys. Rev. A*, vol. 38, no. 4, pp. 2018–2021, 1988.

[9] S. G. Murdoch, R. Leonhardt, and J. D. Harvey, "Polarization modulation instability in weakly birefringent fibers," *Opt. Lett.*, vol. 20, no. 8, pp. 866–868, 1995.

[10] G. Millot, E. Seve, S. Wabnitz, and M. Haelterman, "Observation of induced modulational polarization instabilities and pulse-train generation in the normal-dispersion regime of a birefringent optical fiber," *J. Opt. Soc. Amer. B*, vol. 15, no. 4, pp. 1266–1277, 1998.

[11] S. Trillo and S. Wabnitz, "Bloch wave theory of modulational polarization instabilities in birefringent optical fibers," *Phys. Rev. E*, vol. 56, no. 1, pp. 1048–1058, 1997.

[12] S. Trillo and S. Wabnitz, "Dynamic spontaneous fluorescence in parametric wave coupling," *Phys. Rev. E*, vol. 55, no. 5, pp. R4897–R4900, 1997.

[13] C. De Angelis, M. Santagiustina, and S. Trillo, "Induced modulational instability in high-birefringence fibers: The strong conversion regime," *Opt. Lett.*, vol. 19, no. 5, pp. 335–337, 1994.

[14] C. De Angelis, M. Santagiustina, and S. Trillo, "Four-photon homoclinic instabilities in nonlinear highly birefringent media," *Phys. Rev. E*, vol. 51, no. 1, pp. 774–791, 1995.

[15] E. Seve, G. Millot, and S. Trillo, "Strong four-photon conversion regime of cross-phase-modulation-induced modulational instability," *Phys. Rev. E*, vol. 61, no. 3, pp. 3139–3150, 2000.

[16] G. Millot, S. Pitois, and P. T. Dinda, "Modulational instability processes in optical isotropic fibers under dual-frequency circular polarization pumping," *J. Opt. Soc. Amer. B*, vol. 19, no. 3, pp. 454–460, 2002.

[17] S. Pitois, G. Millot, and S. Wabnitz, "Nonlinear polarization dynamics of counterpropagating waves in an isotropic optical fiber: Theory and experiments," *J. Opt. Soc. Amer. B*, vol. 18, no. 4, pp. 432–443, 2001.

[18] A. L. Berkhoer and V. E. Zakharov, "Self excitation of waves with different polarizations in nonlinear media," *J. Exp. Theor. Phys.*, vol. 31, no. 3, pp. 486–490, 1970.

[19] P. Kockaert, M. Haelterman, S. Pitois, and G. Millot, "Isotropic polarization modulational instability and domain walls in spun fibers," *Appl. Phys. Lett.*, vol. 75, no. 19, pp. 2873–2875, 1999.

[20] H. Zhang, M. Gilles, M. Guasoni, B. Kibler, and A. Picozzi, and J. Fatome, "Isotropic polarization modulational instability in single-mode conventional telecom fibers," *J. Opt. Soc. Amer. B*, vol. 36, no. 19, pp. 2445–2451, 2019.

[21] R. I. Laming and D. N. Payne, "Electric current sensors employing spun highly birefringent optical fibers," *J. Lightwave Technol.*, vol. 7, no. 12, pp. 2084–2094, 1989.
[22] A. J. Barlow, J. J. Ramskov-Hansen, and D. N. Payne, "Birefringence and polarization mode-dispersion in spun single-mode fibers," *Appl. Opt.*, vol. 20, no. 17, pp. 2962–2968, 1981.
[23] D. Kowal *et al.*, "Measurement of birefringence and ellipticity of polarization eigenmodes in spun highly birefringent fibers using spectral interferometry and lateral point-force method," *Opt. Exp.*, vol. 26, no. 26, pp. 34185–34199, 2018.
[24] G. Statkiewicz, T. Martynkien, and W. Urbanczyk, "Measurements of modal birefringence and polarimetric sensitivity of the birefringent holey fiber to hydrostatic pressure and strain," *Opt. Commun.*, vol. 241, no. 4–6, pp. 339–348, 2004.
[25] C. R. Menyuk, "Pulse propagation in an elliptically birefringent KERR medium," *IEEE J. Quantum Electron.*, vol. 25, no. 12, pp. 2674–2682, Dec. 1989.
[26] G. P. Agrawal, "Modulation instability induced by cross-phase modulation," *Phys. Rev. Lett.*, vol. 59, no. 8, pp. 880–883, 1987.
[27] J. E. Rothenberg, "Modulational instability of copropagating frequencies for normal dispersion," *Phys. Rev. Lett.*, vol. 64, no. 7, p. 813, 1990.
[28] J. Fatome, C. Finot, A. Armaroli, and S. Trillo, "Observation of modulationally unstable multi-wave mixing," *Opt. Lett.*, vol. 38, no. 2, pp. 181–183, 2013.
[29] A. Armaroli and S. Trillo, "Collective modulation instability of multiple four-wave mixing," *Opt. Lett.*, vol. 36, no. 11, pp. 1999–2001, 2011.
[30] A. Armaroli and S. Trillo, "Modulational instability due to cross-phase modulation versus multiple four-wave mixing: The normal dispersion regime," *JOSA B*, vol. 31, no. 3, pp. 551–558, 2014.
[31] F. Baronio, M. Conforti, A. Degasperis, S. Lombardo, M. Onorato, and S. Wabnitz, "Vector rogue waves and baseband modulation instability in the defocusing regime," *Phys. Rev. Lett.*, vol. 113, no. 3, pp. 1–5, 2014.
[32] B. Frisquet *et al.*, "Polarization modulation instability in a manakov fiber system," *Phys. Rev. A*, vol. 92, no. 5, pp. 1–8, 2015.
[33] D. Marcuse, C. R. Menyuk, and P. K. A. Wai, "Application of the Manakov-PMD equation to studies of signal propagation in optical fibers with randomly varying birefringence," *J. Light. Technol.*, vol. 15, no. 9, pp. 1735–1745, 1997.
[34] J. M. Dudley, G. Genty, and S. Coen, "Supercontinuum generation in photonic crystal fiber," *Rev. Mod. Phys.*, vol. 78, no. 4, pp. 1135–1184, 2006.